
# Evaluating Nitrogen Use Efficiency in wheat using UAV Multispectral images

***Jie Wang[1], Kang Yu[1*]***

*[1] Precision Agriculture Laboratory, School of Life Sciences, Technical University of Munich, Freising 85354, Germany*

**A paper from the Proceedings of the**
**16th International Conference on Precision Agriculture**
**21-24 July 2024**
**Manhattan, Kansas, United States**

***Abstract.***

*Nitrogen (N) is one of the most important nutrients for crop growth and development. For crops, nitrogen fertilizer is the guarantee of high yield, but in practical applications, nitrogen fertilizer is often excessive. Therefore precise and rapid assessment of nitrogen use efficiency (NUE) plays a pivotal role in optimizing fertilizer utilization and ensuring responsible use of nitrogen in agriculture. While most of research evaluate NUE from management scales, e.g., from the field, district to regional perspectives, and there is no pixel-level spatially-explicit evaluations of NUE using drone images. The objective of this study was to explore the use of UAV multispectral data to directly obtain pixel-level NUE maps in the early stages of wheat growth. We acquired drone multispectral images of the 2022 and 2023 wheat growing seasons at the Freising Experimental Station and extracted spectral features, including texture features, canopy height, and spectral index. Most effective indicators were selected using the combination of random forests and co- correlation analysis. Based on these selected features, different machine learning and deep learning models were used to predict NUE, and the accuracy of these models was evaluated. We identified CH (Canopy height), NGRDI (Normalized green-red difference index), NDREg (Normalized difference red-edge green), and IPCA (Principal component analysis index) as the most predictive indicators for NUE ($r > 0.7$). Additionally, our study revealed the superiority of the Partial Least Squares Regression (PLSR) model, achieving a high coefficient of determination ($R2 > 0.6$) and low running time. Deep learning models (CNN, LSTM, bidirectional LSTM, CNN-RNN) were time-consuming, although they had high and stable determination indices.We compared the features we selected with those used in other studies and found commonalities in estimating NUE features. Results highlighted that the red edge spectral indices and color-band indices were effective in predicting NUE in flowering period and preceding stages. These findings underscore the potential of employing UAV remote sensing techniques for early-stage assessment of nitrogen use efficiency. This study not only enhances our understanding of crop management but also offers practical applications in improving fertilizer utilization and minimizing environmental impact.*

***Keywords.***
*Nitrogen use efficiency, UAV, machine learning, deep learning spectral features*

# 1. Introduction

Nitrogen (N) is one of the most important nutrients for plant growth and development (Jiang et al., 2021). It is essential for the synthesis of amino acids, proteins, and chlorophyll, and therefore, it is crucial for the production of food, feed, and crop (Jensen et al., 2011). In agricultural production, nitrogen fertilizer is the main source of crop growth. To achieve higher yields, excessive nitrogen fertilizer is often applied with detrimental environmental side effects (Chen et al., 2021). Therefore, it is crucial for optimizing nitrogen management in agriculture to achieve high crop yield and quality while minimizing nitrogen losses and environmental pollution.

Nitrogen use efficiency (NUE) is commonly used to monitor and assess the sustainability of nitrogen management. Currently, the calculation of crop NUE mostly relies on field measurements and regional statistical calculations (Duan et al., 2014; Hegedus et al., 2023). These requires a significant amount of people, time, and economic resources, and it may potentially cause destructive impacts on the crops. On the other hand, the results obtained from the latter are too coarse and cannot provide NUE at the within field resolution needed for precise fertilizer application (Gracia-Romero et al., 2020). Meanwhile manual acquisition can only sample specific locations at specific times. A possible solution for acquiring the needed data could be the use of remote sensing at local scales via unmanned aerial vehicles (UAVs). However, there is relatively limited research on directly estimating crop NUE using remote sensing data, especially utilizing UAVs to acquire NUE at millimetre-level or centimetre-level spatial resolutions.

Kefauver et al. (2017) used vegetation indices to evaluate NUE in barley and were able to explain up to 83% of total NUE variability by combining UAV and field-based measurements. This directly demonstrates the feasibility of using drones for remote sensing-based NUE calculations. Yang et al. (2020) found that NDRE, which was extracted using a multispectral camera mounted on the drone, could predict NUE with a consistently high accuracy, especially in the later stages of grain filling. Jiang et al. (2021) utilized UAV and scanner to quickly obtain high spatial resolution NUE data for rice fields using NDVI and They believe that NDVI measurement is an effective method to evaluate NUE during nutrient-sensitive growth stages, especially the tillering and panicle stages. Liu et al. (2022) predicted NUE and yield using vegetation indices independent of the growth period and three regression methods, with high predictive ability for yield but only moderate predictive ability for NUE. In general, despite the advanced state of remote sensing and drone technologies, research directly assessing crop NUE using drones remains very limited. Most of the aforementioned studies are based on yield or biomass estimation, with NUE serving merely as an explanatory indicator. Meanwhile, the relationship between multispectral bands information and NUE estimation has not been thoroughly investigated. The majority of studies directly employ commonly used vegetation indices (NDVI, NDRE, etc.) without exploring the effectiveness of other indices or identifying commonalities among indices that are effective for NUE estimation.

We investigated the potential of using drone-based remote sensing to predict nitrogen use efficiency during the growing season using experimental plots grown with wheat on different plots in Freising. Our goals are: (1) to use UAV multispectral data to directly obtain pixel-level NUE maps in the early stages of wheat growth; (2) to find commonalities in spectral features for estimating NUE.

# 2. Methods

## 2.1 Field work

*Experimental design*

The experimental site is located at the Dürnast experimental station in Freisng (48.4037°N, 11.7056°E). The region has a temperate climate with an average annual precipitation of approximately 946 mm and an annual average temperature of 10.2 °C (Dietzel et al. 2023). The experiment was established in 2021 as part of the multisite experiment LegacyNet

(https://legacynet.scss.tcd.ie/) and involved 60 plots, with each plot measuring 7m × 3m in size (Fig 1(a)). Wheat was planted in 2022 and 2023, and soil Nmin was measured before wheat sowing. The experiment kept nitrogen fertilizer application low during the growth period of spring wheat applying ammonium hydrate solution 25 kg/ha late during the growth at the booting stage (June).


**Fig 1. Distribution of the Experimental design**

*Yield measurement*

We used a combine harvester to harvest the plots and obtained grain samples from each plot at the same time. After harvesting, we obtained the final grain yield (threshing, drying, etc.) of 60 plots. We used an elemental analyser to get the nitrogen concentration of wheat grains after drying. We calculated grain nitrogen content by multiplying grain yield by nitrogen concentration.

## 2.2 NUE calcuation

Nitrogen use efficiency (NUE) represents the ability of a crop to absorb nitrogen from applied nitrogen and convert the absorbed nitrogen into grain (Mălinaş et al. 2022). In this study, we utilized two methods to calculate NUE.

The first method of NUE is defined as the grain yield produced per unit of applied nitrogen fertilizer and is also known as partial factor productivity (PFP) (Ghafoor et al. 2021). The second method of NUE is defined as the ratio of grain nitrogen content to the total input nitrogen content and is also known as partial nitrogen balance (PNB) (Yingxia Liu et al. 2020).

$$\mathrm{PNB} = \mathrm{N_{Grain}}/(\mathrm{N_{fert}} + \mathrm{Nmin}) \quad (1)$$

$$\mathrm{PFP} = \mathrm{Yield}/(\mathrm{N_{fert}} + \mathrm{Nmin}) \quad (2)$$

Where $N_{Grain}$ is the nitrogen content of the crop grain. $N_{fert}$ is the amount of nitrogen fertilizer applied. Yield is crop grain yield. $N_{min}$ is the soil mineral nitrogen.

## 2.3 UAV multispectral data

From wheat booting stage to senescence stage, we collected UAV multispectral images in 2022 and 2023 (Table 1). We used Matrice M300 drones carried on micasense camera. The flying height of the M300 was 25m.The basic processing of UAV images, including splicing, correction, calibration and other processes, was carried out in Aigsoft.

**Table 1. UAV Image Acquisition Information**

| Date | Measurenment | BBCH | Stage |
|---|---|---|---|

| | | | |
|---|---|---|---|
| 6/10/2022 | Micasense 300 | 49 | Booting |
| 6/17/2022 | Micasense 300 | 56 | Heading |
| 6/22/2022 | Micasense 300 | 61 | Flowering |
| 7/18/2022 | Micasense 300 | 87 | Ripening |
| 5/18/2023 | Micasense 300 | 47 | Booting |
| 6/15/2023 | Micasense 300 | 58 | Heading |
| 6/21/2023 | Micasense 300 | 65 | Flowering |
| 7/11/2023 | Micasense 300 | 83 | Ripening |

Note: BBCH-scales have been developed for a range of crop species where similar growing stage of each plant are given the same code. For wheat, 40-49 is booting stage, 50-59 is heading stage, 60-69 is flowering stage, 70-79 is milk stage, 80-89 is ripening stage, 90-99 is senescence stage.

We calculated spectral features including textural features, spectral index and canopy height at different growing stages.

*Texture features*

We first calculated the four relative directions (θ = 0°, 45°, 90° and 135°) texture feature; the relative distance used to pair with each direction is a uniform distance (d = 1). Secondly, we calculated the average value of the 4 directions as the final texture feature of the sample. In this study, we selected contrast, dissimilarity, homogeneity, correlation, angular second moment as texture features (Table 2). Multispectral bands (R, G, B, RE, NIR) are evaluated using these five texture features. The entire texture calculation process is completed in python.

**Table 2. The grey-level co-occurrence matrix (GLCM) textural features used in this study**

| Texture | Description | Equation |
|---|---|---|
| Contrast | Measures the local variations in the gray-level co-occurrence matrix. Higher contrast values indicate a greater difference between the values of adjacent pixels. | $\sum_{x=1}^{G}\sum_{y=1}^{G}(x-y)^2P(x,y)$ |
| Dissimilarity | Measures the differences between adjacent pixel values in the gray-level co-occurrence matrix. | $\sum_{x=1}^{G}\sum_{y=1}^{G}P(x,y)\lvert x-y\rvert$ |
| Homogeneity | Measures the closeness of the distribution of elements in the gray-level co-occurrence matrix to the diagonal. Higher homogeneity values indicate that the values of adjacent pixels are more similar. | $\sum_{x=1}^{G}\sum_{y=1}^{G}\frac{P(x,y)}{1+(x-y)^2}$ |
| Correlation | Measures the linear dependency between gray-level co-occurrence matrix elements. | $\sum_{x=1}^{G}\sum_{y=1}^{G}\frac{(x-y)(y-x)P(x,y)}{\sqrt{ASM_x}\sqrt{ASM_y}}$ |
| Angular second moment (ASM) | Also called uniformity, measures the homogeneity or uniformity of the gray-level co-occurrence matrix | $\sum_{x=1}^{G}\sum_{y=1}^{G}(x-\mu)^2P(x,y)$ |

Note: In the equations, x and y represent the row number and column number of the image, respectively; P(x, y) represents the relative frequency of two neighboring pixels.

*Canopy Height*

We derived canopy height by subtracting the Digital Elevation Model (DEM) from the Digital Surface Model (DSM) generated from RGB images. The canopy height model (CHM) established from this is a commonly used and effective method for obtaining crop canopy height (Maimaitijiang et al. 2020).

*Spectral index*

In this study we calculated 16 color-band indices (using only RGB bands) and 16 vegetation indices (Table 3). Considering the UAV's multi-spectral bands (blue band, green band, red band, red edge, near-infrared), there are a total of 37 spectral indices for each growing stage.

**Table 3. The spectral indices used in this study**

| Type | Index | Description | Equation | References |
|---|---|---|---|---|
| Color-band indices | BCC | Blue chromatic coordinate | $B/(R+G+B)$ | (Zeng et al. 2021) |
| | GCC | Green chromatic coordinate | $G/(R+G+B)$ | (Zeng et al. 2021) |
| | RCC | Red chromatic coordinate | $R/(R+G+B)$ | (Ying Liu et al. 2020) |
| | GRRI | Green–red ratio index | $G/R$ | (Maimaitijiang et al. 2019) |
| | GBRI | Green–blue ratio index | $G/B$ | (Maimaitijiang et al. 2019) |
| | RBRI | Red–blue ratio index | $R/B$ | (Maimaitijiang et al. 2019) |
| | NGRDI | Normalized green-red difference index | $(G-R)/(G+R)$ | (Tucker 1979) |
| | WI | Woebbecke index | $(G-B)/(R-G)$ | (Woebbecke et al. 1995) |
| | IKAW | Kawashima index | $(R-B)/(R+B)$ | (KAWASHIMA and NAKATANI 1998) |
| | GLI | Green leaf index | $(2\times G-R-B)/(2\times G+R+B)$ | (Louhaichi et al. 2001) |
| | VARI | Visible atmospherically resistance index | $(G-R)/(G+R-B)$ | (Gitelson et al. 2002) |
| | EXR | Excess red vegetation index | $1.4\times RCC-GCC$ | (Wenhua Mao et al. 2003) |
| | EXG | Excess green vegetation index | $2\times GCC-RCC-BCC$ | (Wenhua Mao et al. 2003) |
| | EXB | Excess blue vegetation index | $1.4\times BCC-GCC$ | (Wenhua Mao et al. 2003) |
| | IPCA | Principal component analysis index | $0.994\times\lvert R-B\rvert+0.961\times\lvert G-B\rvert+0.914\times\lvert G-R\rvert$ | (Saberioon et al. 2014) |
| | CIVE | Color index of vegetation | $0.441\times R-0.881+0.385\times B+18.79$ | (Kataoka et al. 2003) |
| Vegetation indices | RVI | Ratio vegetation index | $NIR/R$ | (Tucker 1979) |
| | GCI | Green chlorophyll index | $(NIR/G)-1$ | (Gitelson et al. 2005) |
| | RECI | Red-edge chlorophyll index | $(NIR/RE)-1$ | (Gitelson et al. 2005) |
| | NDVI | Normalized difference vegetation index | $(NIR-R)/(NIR+R)$ | (Freden et al. 1974) |
| | GNDVI | Green normalized difference vegetation index | $(NIR-G)/(NIR+G)$ | (Gitelson et al. 2003) |
| | NDRE | Normalized difference red-edge | $(NIR-RE)/(NIR+RE)$ | (Gitelson et al. 2005) |
| | NDREg | Normalized difference red-edge green | $(RE-G)/(RE+G)$ | (Hassan et al. 2018) |
| | SCCCI | Simplified canopy chlorophyll content index | $NDRE/NDVI$ | (Raper and Varco 2015) |
| | EVI | The enhanced vegetation index | $2.5\times(NIR-R)/(1+NIR-2.4\times R)$ | (Huete et al. 2002) |
| | EVI2 | Two-band enhanced vegetation index | $2.5\times(NIR-R)/(1+NIR+2.4\times R)$ | (Jiang et al. 2008) |
| | OSAVI | Optimized soil adjusted vegetation index | $(NIR-R)/(NIR-R+L)(L=0.16)$ | (Rondeaux et al. 1996) |
| | MCARI | Modified chlorophyll absorption in reflectance index | $[(RE-R)-0.2\times(RE-G)]\times(RE/R)$ | (Daughtry et al. 2000) |
| | TCARI | Transformed chlorophyll absorption in reflectance index | $3\times[(RE-R)-0.2\times(RE-G)\times(RE/R)]$ | (Haboudane et al. 2002) |
| | MCARI/OSAVI | | MCARI/OSAVI | (Daughtry et al. 2000) |
| | TCARI/OSAVI | | TCARI/OSAVI | (Haboudane et al. 2002) |
| | WDRVI | Wide dynamic range vegetation index | $(a\times NIR-R)/(a\times NIR+R)(a=0.12)$ | (Gitelson 2004) |

## 2.4 Data analysis

In this study, feature selection was performed to identify optimal features (spectral indices, texture features, and canopy height model) for evaluating wheat NUE. Next, machine learning and deep learning models were trained to predict NUE. Ultimately, a high-resolution NUE spatial distribution map was generated using the best machine learning model (Fig 2).

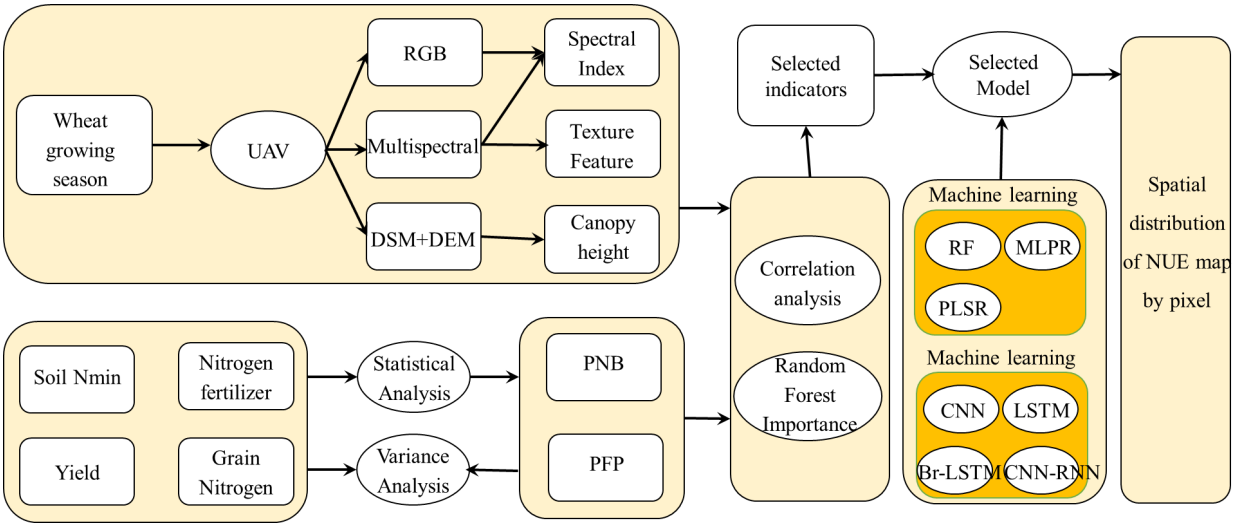


**Fig 3. Workflow of this study**

*Feature selection*

We used correlation and random forest feature importance at the same time to obtain optimal features that are more effective in NUE prediction (Fig 3). We first used random forest to calculate the feature importance on different dates for the features calculated from UAV images, then selected the top 3 features with the highest importance in each stage, named stage specific top features. Next, we calculated the correlation between NUE and the stage specific top features to reduce the collinearity and reduce overfitting (Zhao et al. 2022), and finally obtain a small number of the general optimal features.

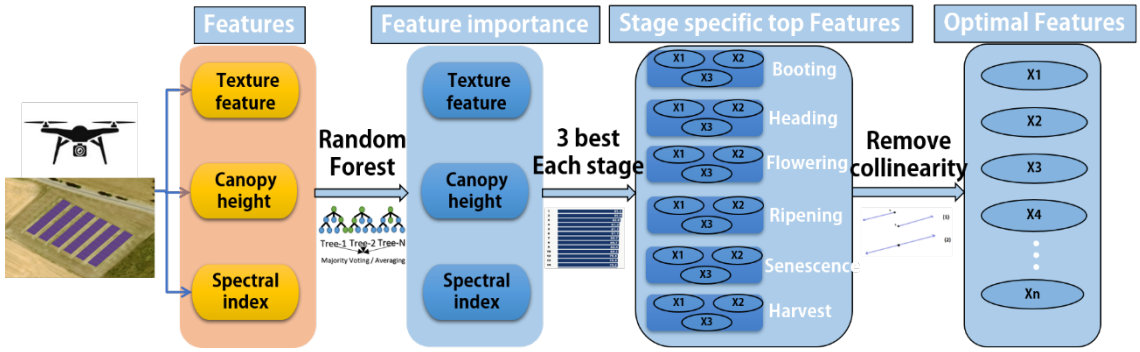


**Fig 3. Workflow of feature selection**

*Model selection*

We used machine learning and deep learning to evaluate the performance of selected features in estimating wheat nitrogen use efficiency. In this study, we used random forest regression (RF), partial least squares regression (PLSR), multilayer perceptron regression (MLPR), single-layer Convolutional Neural Network (CNN), Long Short-Term Memory (LSTM), bidirectional LSTM (Bi-LSTM), and CNN-RNN models (Table 4). Models were implemented in Python using the sklearn and TensorFlow library.

**Table 4. Description of different models**

| Model | Input data |
|---|---|
| Random forest (RF) | 2022-2023 one stage features |
| Partial least squares regression (PLSR) | 2022-2023 one stage features |
| Multilayer perceptron regression (MLPR) | 2022-2023 one stage features |
| Single-layer Convolutional Neural Network (CNN) | 2022-2023 one stage features |

| | |
|---|---|
| Long Short-Term Memory (LSTM) | 2022-2023 heading and flowering features |
| bidirectional LSTM | 2022-2023 heading and flowering features |
| CNN-RNN | 2022-2023 heading and flowering features |

In this study, we randomly split the data into training and validation sets with 7:3. We select Explained Variance, Mean Absolute Error (MAE), Root Mean Squared Error (RMSE), R-squared ($R^2$), and runtime as evaluation metrics.

# 3. Results

## 3.1 Optimal features selection results

From Fig 4, we can get the stage specific top features including NDI, RBRI, NDREg, RCC, EXR, CH, CIVE, IPCA.

Considering the extremely high linear correlations (|r| > 0.9) among EVI, EVI2, NIR, GNDVI, OSAVI, NDREg at heading and flowering stage (Fig 5), and also the redundancy among RCC, BCC, RBRI, NGRDI, and EXR (|r| > 0.9), the following 4 optimal features were finally determined for NUE calculation: CH, NGRDI, NDREg, IPCA.

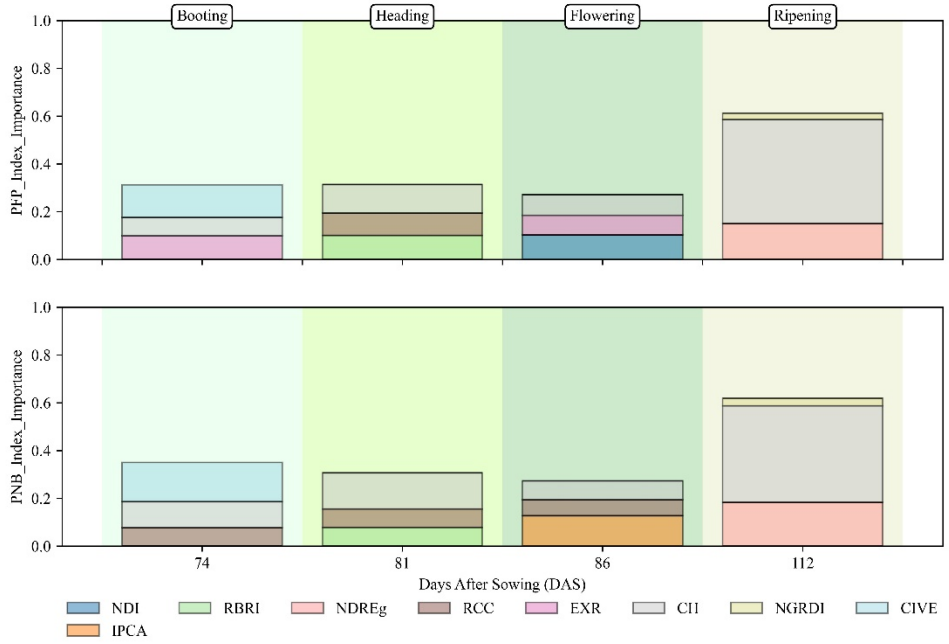


**Fig 4. The stage specific top featues of of different growing stage**

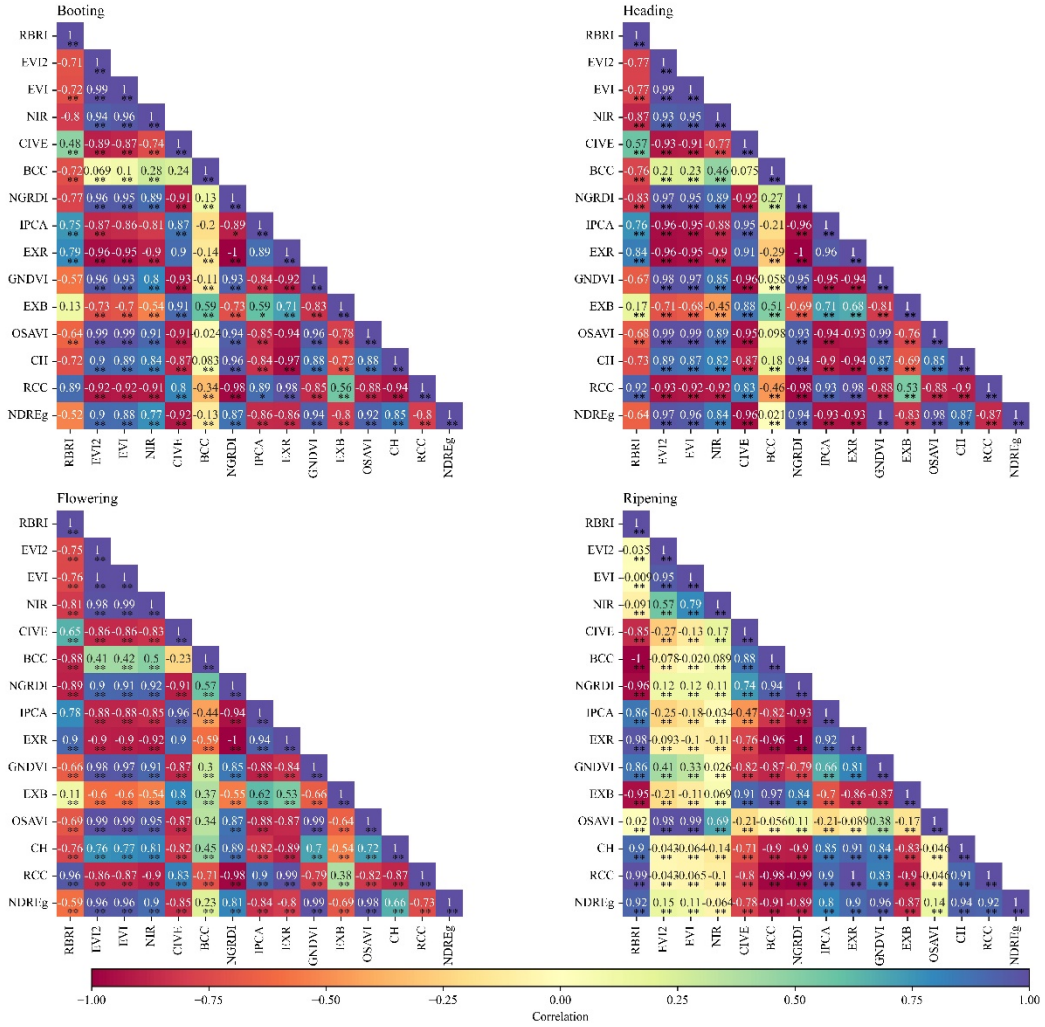


**Fig 5. Correlation between important indicators at different growing stage**

## 3.2 Comparing Models for NUE prediction

According to Table 5, the R2 values of most models exceeded 0.5, indicating that these models can explain more than 50% of the variation in PFP. The R2 value of PLSR was 0.62, the highest among all models, indicating that it had the best prediction effect on PFP. Other models with good performance included CNN-RNN (R2 = 0.61) and LSTM (R2 = 0.58). PLS regression and random forest had the shortest training time, which were 0.15 and 0.14 seconds, respectively. Deep learning models such as CNN-RNN and BiLSTM took longer to train, especially CNN-RNN, which required 78.95 seconds.

Similarly, the R2 values of most models in PNB prediction exceeded 0.7, indicating that these models had good fitting effects in the early stage of wheat growth. The training time of PLSR was the shortest, almost zero, indicating that it had the highest computational efficiency. The R2 value of random forest was 0.80, the highest among all models.

In general, PLSR and random forest are good choices for high accuracy and short training time. For scenarios that require higher prediction accuracy, CNN-RNN can be considered, but the longer training time must be weighed.

**Table 5. NUE (PFP) Models Validation Accuracy**

| Model | MAE | RMSE | R2 | Training Time |
|---|---|---|---|---|

| | | | | |
|---|---|---|---|---|
| Random Forest | 10.61 | 14.66 | 0.54 | 0.14 |
| PLSR | 10.62 | 13.35 | 0.62 | 0.15 |
| MLPR | 11.33 | 15.37 | 0.50 | 0.30 |
| Single-layer CNN | 10.84 | 14.52 | 0.55 | 17.55 |
| LSTM | 11.29 | 14.11 | 0.58 | 34.12 |
| BiLSTM | 10.86 | 14.19 | 0.57 | 61.20 |
| CNN-RNN | 10.46 | 13.54 | 0.61 | 78.95 |

**Table 6. NUE (PNB) Models Validation Accuracy**

| Model | MAE | RMSE | R2 | Training Time |
|---|---|---|---|---|
| Random Forest | 0.19 | 0.26 | 0.80 | 0.14 |
| PLS Regression | 0.23 | 0.32 | 0.71 | 0.00 |
| MLP Regressor | 0.42 | 0.50 | 0.29 | 0.08 |
| Single-layer CNN | 0.23 | 0.30 | 0.74 | 21.36 |
| LSTM | 0.24 | 0.32 | 0.71 | 36.63 |
| BiLSTM | 0.24 | 0.31 | 0.71 | 52.98 |
| CNN-RNN | 0.23 | 0.30 | 0.74 | 72.27 |

### 3.3 Mapping NUE at pixel-level

We computed the spatial distribution of wheat NUE at flowering stage on 2022 using PLSR model (Fig 6). We found that the spatial distribution characteristics of NUE (PNB) and NUE (PFP) did not differ significantly. The marginal differences were primarily due to the distinct calculation methods of the two NUE indicators.

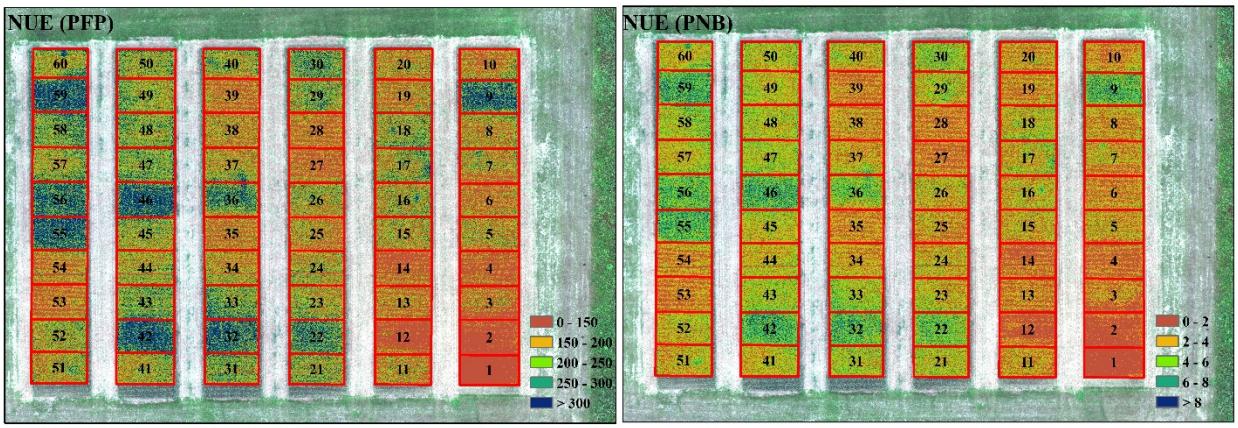


**Fig 6. Wheat NUE-by-pixel distribution prediction at flowering stage on 2022**

# 4. Discussion

## 4.1 Importance of red-edge spectral indices

It is worth noting that those spectral indices showed close correlations with NUE are mainly related to chlorophyll and canopy structure - for example, NDVI, GNDVI, NDRE, NDREg, MTCI and RECI, which have been commonly used in previous studies (Jiang et al. 2008; J. Liu et al. 2022; Pavuluri et al. 2015; Yang et al. 2020).

Among those indices, NDRE, NDREg, RECI, and MTCI all involve the red-edge wavelength region and are used to assess crop health and canopy chlorophyll content. The RE (red-edge)

band captures the transition zone between red and infrared light, providing valuable information about canopy structure. The red-edge spectrum is typically between 680 and 750 nanometers. The interaction between vegetation and sunlight in this spectral interval provides subtle information about the health, density and arrangement of plant leaves. It has been found to be important for crop canopy information (chlorophyll and nitrogen) (Li et al. 2014). Changes in canopy structure, such as Leaf Area Index and crop height, can indicate plant responses to nitrogen availability (Yang Liu et al. 2021).

The correlations between MTCI, NDRE, NDREg and RECI were high, resulting in potential data redundancy if all are used simultaneously in a model. Therefore we'd better choose one of these indices in the final model. The differences in calculation bands and usage scenarios of these indices are mainly reflected in the following aspects. Both NDRE and RECI include NIR (Near-Infrared), which is sensitive to water content in plant tissues. Variations in water content can impact NIR signals, potentially confounding nitrogen content estimates. This interference might lead to inaccuracies in assessing wheat NUE, especially in environments with fluctuating water resources. Meanwhile, the sensitivity of NIR at low nitrogen levels is limited, and it easily saturates at high nitrogen levels (Sharma and Bali 2018). MTCI (MERIS Terrestrial Chlorophyll Index) takes advantage of the fact that the chlorophyll absorption characteristics in the red edge region (around 709nm) are sensitive to the chlorophyll content in plants. Taking into account soil background reflectance, adding reflectance at 754 nm and 681 nm allows for a more accurate estimate (Dash and Curran 2007). MTCI is considered more applicable to a wider range of crops as it attempts to minimize the effects of changes in soil reflectivity, making it more robust across different soil types and vegetation conditions (Dash and Curran 2007). NDREg emphasizes vegetation cover, as well as vegetation structure and quantity, potentially performing well in specific crop types. Therefore, the selection of MTCI and NDREg can be determined based on crop type and nitrogen performance.

### 4.2 Importance of Color-band only spectral indices

NDVI, GNDVI, and NGRDI are the common type of “normalized difference indices” for estimating crop coverage and can reflect canopy differences in response to nitrogen supply and crop yield. The three indices differ in their bands (Table 4), NDVI emphasizes NIR and R, GNDVI emphasizes NIR and G, and NGRDI emphasizes R and G. NGRDI outperforms NDVI in identifying vegetation in low nitrogen treatment, while NDVI excels vegetation in high nitrogen treatment, albeit encountering saturation issues in the later growth stages (Maresma et al. 2016). Both NGRDI and GNDVI emphasize the green band, but NGRDI is more suitable for green crops, while GNDVI highlights near-infrared, making it applicable to a broader range of crops, but near-infrared is not sensitive to vegetation of low nitrogen treatment and always influenced by water content (Hunt et al. 2018). In our study, we observed that before and during the flowering stage, GNDVI and NDVI exhibited a strong correlation of 0.99, which weakened in subsequent stages. The correlation between GNDVI and NGRDI was also strong. To avoid data redundancy, either of these two can be selected.

These color indices can be obtained using standard digital cameras or portable spectrometers, reducing costs, especially for small-scale farmers. Moreover, the intuitive nature of color indices allows farmers and non-professionals to comprehend and utilize the results effectively.

## 5. Conclusions

We explored the potential of using UAV multispectral data to predict variations in wheat NUE using two year data. To this end, we identified four spectral indices based on machine learning and deep learining models (including CH, NGRDI, NDREg, IPCA) that demonstrated strong performance in predicting NUE (validation R2 > 0.5). PLSR and random forest have high fitting accuracy and short running time. Deep learning model has stable fitting accuracy but is time-consuming. Additionally, we discovered the advantages and potential of the red-edge index and

color band index in predicting NUE.

**Acknowledgments**

We acknowledge use of the experimental design and elements of the sampling protocol developed by LegacyNet (https://legacynet.scss.tcd.ie/), and thank Wolfgang Heer and the field crop unit of the plant technology center of the Technical University of Munich for setting-up and running the field site. We thank Laura Argens and Sarah Sturm (Terrestrial Ecology Research group) for support in running the field measurements. Thanks to technician Jürgen Plass and master students Subash Sedai, Gao Yu, Yidan Wang for their help with AUV data collection. Thanks to Robert Kahle and his laboratory staff for their contribution to the nitrogen concentration measurements. This study was supported by the Deutsche Forschungsgemeinschaft (DFG) through the TUM International Graduate School of Science and Engineering (IGSSE, GSC 81) as part of the International Project 13.10: EcoServ, and the China Scholarship Council (No. 202106810011).

## References

Dash, J., & Curran, P. J. (2007). Evaluation of the MERIS terrestrial chlorophyll index (MTCI). Advances in Space Research, 39(1), 100–104. https://doi.org/10.1016/j.asr.2006.02.034

Daughtry, C. S. T., Walthall, C. L., Kim, M. S., de Colstoun, E. B., & McMurtrey, J. E. (2000). Estimating Corn Leaf Chlorophyll Concentration from Leaf and Canopy Reflectance. Remote Sensing of Environment, 74(2), 229–239. https://doi.org/10.1016/S0034-4257(00)00113-9

Dietzel, S., Rojas-Botero, S., Kollmann, J., & Fischer, C. (2023). Enhanced urban roadside vegetation increases pollinator abundance whereas landscape characteristics drive pollination. Ecological Indicators, 147, 109980. https://doi.org/10.1016/j.ecolind.2023.109980

Freden, S. C., Mercanti, E. P., & Becker, M. A. (1974). Third Earth Resources Technology Satellite-1 Symposium: The Proceedings of a Symposium Held by Goddard Space Flight Center at Washington, D.C. on December 10-14, 1973 : Prepared at Goddard Space Flight Center. Scientific and Technical Information Office, National Aeronautics and Space Administration.

Ghafoor, I., Habib-ur-Rahman, M., Ali, M., Afzal, M., Ahmed, W., Gaiser, T., & Ghaffar, A. (2021). Slow-release nitrogen fertilizers enhance growth, yield, NUE in wheat crop and reduce nitrogen losses under an arid environment. Environmental Science and Pollution Research, 28(32), 43528–43543. https://doi.org/10.1007/s11356-021-13700-4

Gitelson, A. A. (2004). Wide Dynamic Range Vegetation Index for Remote Quantification of Biophysical Characteristics of Vegetation. Journal of Plant Physiology, 161(2), 165–173. https://doi.org/10.1078/0176-1617-01176

Gitelson, A. A., Gritz †, Y., & Merzlyak, M. N. (2003). Relationships between leaf chlorophyll content and spectral reflectance and algorithms for non-destructive chlorophyll assessment in higher plant leaves. Journal of Plant Physiology, 160(3), 271–282. https://doi.org/10.1078/0176-1617-00887

Gitelson, A. A., Kaufman, Y. J., Stark, R., & Rundquist, D. (2002). Novel algorithms for remote estimation of vegetation fraction. Remote Sensing of Environment, 80(1), 76–87. https://doi.org/10.1016/S0034-4257(01)00289-9

Gitelson, A. A., Viña, A., Ciganda, V., Rundquist, D. C., & Arkebauer, T. J. (2005). Remote estimation of canopy chlorophyll content in crops. Geophysical Research Letters, 32(8). https://doi.org/10.1029/2005GL022688

Haboudane, D., Miller, J. R., Tremblay, N., Zarco-Tejada, P. J., & Dextraze, L. (2002). Integrated narrow-band vegetation indices for prediction of crop chlorophyll content for application to precision agriculture. Remote Sensing of Environment, 81(2), 416–426. https://doi.org/10.1016/S0034-4257(02)00018-4

Hassan, M. A., Yang, M., Rasheed, A., Jin, X., Xia, X., Xiao, Y., & He, Z. (2018). Time-Series Multispectral Indices from Unmanned Aerial Vehicle Imagery Reveal Senescence Rate in Bread Wheat. Remote Sensing, 10(6), 809. https://doi.org/10.3390/rs10060809

Huete, A., Didan, K., Miura, T., Rodriguez, E. P., Gao, X., & Ferreira, L. G. (2002). Overview of the radiometric and biophysical performance of the MODIS vegetation indices. Remote Sensing of Environment, 83(1), 195–213. https://doi.org/10.1016/S0034-4257(02)00096-2

Hunt, E. R., Horneck, D. A., Spinelli, C. B., Turner, R. W., Bruce, A. E., Gadler, D. J., et al. (2018). Monitoring nitrogen status of potatoes using small unmanned aerial vehicles. Precision Agriculture, 19(2), 314–333. https://doi.org/10.1007/s11119-017-9518-5

Jiang, Z., Huete, A. R., Didan, K., & Miura, T. (2008). Development of a two-band enhanced vegetation index without a blue band. Remote Sensing of Environment, 112(10), 3833–3845. https://doi.org/10.1016/j.rse.2008.06.006

Kataoka, T., Kaneko, T., Okamoto, H., & Hata, S. (2003). Crop growth estimation system using machine vision. In Proceedings 2003 IEEE/ASME International Conference on Advanced Intelligent Mechatronics (AIM 2003) (Vol. 2, pp. b1079-b1083 vol.2). Presented at the Proceedings 2003 IEEE/ASME International Conference on Advanced Intelligent Mechatronics (AIM 2003). https://doi.org/10.1109/AIM.2003.1225492

KAWASHIMA, S., & NAKATANI, M. (1998). An Algorithm for Estimating Chlorophyll Content in Leaves Using a Video Camera. Annals of Botany, 81(1), 49–54. https://doi.org/10.1006/anbo.1997.0544

Li, F., Miao, Y., Feng, G., Yuan, F., Yue, S., Gao, X., et al. (2014). Improving estimation of summer maize nitrogen status with red edge-based spectral vegetation indices. Field Crops Research, 157, 111–123. https://doi.org/10.1016/j.fcr.2013.12.018

Liu, J., Zhu, Y., Tao, X., Chen, X., & Li, X. (2022). Rapid prediction of winter wheat yield and nitrogen use efficiency using consumer-grade unmanned aerial vehicles multispectral imagery. Frontiers in Plant Science, 13. https://www.frontiersin.org/articles/10.3389/fpls.2022.1032170. Accessed 11 April 2023

Liu, Yang, Yang, M., Yao, C., Zhou, X., Li, W., Zhang, Z., et al. (2021). Optimum Water and Nitrogen Management Increases Grain Yield and Resource Use Efficiency by Optimizing Canopy Structure in Wheat. Agronomy, 11(3), 441. https://doi.org/10.3390/agronomy11030441

Liu, Ying, Wu, C., Sonnentag, O., Desai, A. R., & Wang, J. (2020). Using the red chromatic coordinate to characterize the phenology of forest canopy photosynthesis. Agricultural and Forest Meteorology, 285–286, 107910. https://doi.org/10.1016/j.agrformet.2020.107910

Liu, Yingxia, Heuvelink, G. B. M., Bai, Z., He, P., Xu, X., Ma, J., & Masiliūnas, D. (2020). Space-time statistical analysis and modelling of nitrogen use efficiency indicators at provincial scale in China. European Journal of Agronomy, 115, 126032. https://doi.org/10.1016/j.eja.2020.126032

Louhaichi, M., Borman, M., & Johnson, D. (2001). Spatially Located Platform and Aerial Photography for Documentation of Grazing Impacts on Wheat. Geocarto International, 16. https://doi.org/10.1080/10106040108542184

Maimaitijiang, M., Sagan, V., Sidike, P., Hartling, S., Esposito, F., & Fritschi, F. B. (2020). Soybean yield prediction from UAV using multimodal data fusion and deep learning.

Remote Sensing of Environment, 237, 111599. https://doi.org/10.1016/j.rse.2019.111599

Maimaitijiang, M., Sagan, V., Sidike, P., Maimaitiyiming, M., Hartling, S., Peterson, K. T., et al. (2019). Vegetation Index Weighted Canopy Volume Model (CVMVI) for soybean biomass estimation from Unmanned Aerial System-based RGB imagery. ISPRS Journal of Photogrammetry and Remote Sensing, 151, 27–41. https://doi.org/10.1016/j.isprsjprs.2019.03.003

Mălinaş, A., Vidican, R., Rotar, I., Mălinaş, C., Moldovan, C. M., & Proorocu, M. (2022). Current Status and Future Prospective for Nitrogen Use Efficiency in Wheat (Triticum aestivum L.). Plants, 11(2), 217. https://doi.org/10.3390/plants11020217

Maresma, Á., Ariza, M., Martínez, E., Lloveras, J., & Martínez-Casasnovas, J. A. (2016). Analysis of Vegetation Indices to Determine Nitrogen Application and Yield Prediction in Maize (Zea mays L.) from a Standard UAV Service. Remote Sensing, 8(12), 973. https://doi.org/10.3390/rs8120973

Pavuluri, K., Chim, B. K., Griffey, C. A., Reiter, M. S., Balota, M., & Thomason, W. E. (2015). Canopy spectral reflectance can predict grain nitrogen use efficiency in soft red winter wheat. Precision Agriculture, 16(4), 405–424. https://doi.org/10.1007/s11119-014-9385-2

Raper, T. B., & Varco, J. J. (2015). Canopy-scale wavelength and vegetative index sensitivities to cotton growth parameters and nitrogen status. Precision Agriculture, 16(1), 62–76. https://doi.org/10.1007/s11119-014-9383-4

Rondeaux, G., Steven, M., & Baret, F. (1996). Optimization of soil-adjusted vegetation indices. Remote Sensing of Environment, 55(2), 95–107. https://doi.org/10.1016/0034-4257(95)00186-7

Saberioon, M. M., Amin, M. S. M., Anuar, A. R., Gholizadeh, A., Wayayok, A., & Khairunniza-Bejo, S. (2014). Assessment of rice leaf chlorophyll content using visible bands at different growth stages at both the leaf and canopy scale. International Journal of Applied Earth Observation and Geoinformation, 32, 35–45. https://doi.org/10.1016/j.jag.2014.03.018

Sharma, L. K., & Bali, S. K. (2018). A Review of Methods to Improve Nitrogen Use Efficiency in Agriculture. Sustainability, 10(1), 51. https://doi.org/10.3390/su10010051

Tucker, C. J. (1979). Red and photographic infrared linear combinations for monitoring vegetation. Remote Sensing of Environment, 8(2), 127–150. https://doi.org/10.1016/0034-4257(79)90013-0

Wenhua Mao, Yiming Wang, & Yueqing Wang. (2003). Real-time Detection of Between-row Weeds Using Machine Vision. In 2003, Las Vegas, NV July 27-30, 2003. Presented at the 2003, Las Vegas, NV July 27-30, 2003, American Society of Agricultural and Biological Engineers. https://doi.org/10.13031/2013.15381

Woebbecke, D. M., Meyer, G. E., Von Bargen, K., & Mortensen, D. A. (1995). Color indices for weed identification under various soil, residue, and lighting conditions. Transactions of the ASABE, 38(1), 259–269.

Yang, M., Hassan, M. A., Xu, K., Zheng, C., Rasheed, A., Zhang, Y., et al. (2020). Assessment of Water and Nitrogen Use Efficiencies Through UAV-Based Multispectral Phenotyping in Winter Wheat. Frontiers in Plant Science, 11. https://www.frontiersin.org/articles/10.3389/fpls.2020.00927. Accessed 11 April 2023

Zeng, L., Peng, G., Meng, R., Man, J., Li, W., Xu, B., et al. (2021). Wheat Yield Prediction Based on Unmanned Aerial Vehicles-Collected Red–Green–Blue Imagery. Remote Sensing, 13(15), 2937. https://doi.org/10.3390/rs13152937

Zhao, Y., Zhu, W., Wei, P., Fang, P., Zhang, X., Yan, N., et al. (2022). Classification of Zambian

grasslands using random forest feature importance selection during the optimal phenological period. Ecological Indicators, 135, 108529. https://doi.org/10.1016/j.ecolind.2021.108529